

Nonlinear finite element analysis of high strength concrete slabs

M. M. Smadi[†] and K. A. Belakhdar

*Department of Civil Engineering, Faculty of Engineering, Jordan University of Science and Technology,
P.O. Box (3030) Irbid 22110, Jordan
(Received September 18, 2006, Accepted May 2, 2007)*

Abstract. A rational three-dimensional nonlinear finite element model is described and implemented for evaluating the behavior of high strength concrete slabs under transverse load. The concrete was idealized by using twenty-nodded isoparametric brick elements with embedded reinforcements. The concrete material modeling allows for normal (NSC) and high strength concrete (HSC), which was calibrated based on experimental data. The behavior of concrete in compression is simulated by an elastoplastic work-hardening model, and in tension a suitable post-cracking model based on tension stiffening and shear retention models are employed. The nonlinear equations have been solved using the incremental iterative technique based on the modified Newton-Raphson method. The FE formulation and material modeling is implemented into a finite element code in order to carry out the numerical study and to predict the behavior up to ultimate conditions of various slabs under transverse loads. The validity of the theoretical formulations and the program used was verified through comparison with available experimental data, and the agreement has proven to be very good. A parametric study has been also carried out to investigate the influence of different material and geometric properties on the behavior of HSC slabs. Influencing factors, such as concrete strength, steel ratio, aspect ratio, and support conditions on the load-deflection characteristics, concrete and steel stresses and strains were investigated.

Keywords: nonlinear analysis; finite element method; reinforced concrete slabs; ultimate strength; high strength concrete; stress-strain relationships; tension stiffening.

1. Introduction

Reinforced concrete slabs are one of the important elements in most structural systems; they are relatively thin structural element, whose main function is to transmit the vertical loading to their supports. Flat plates or beamless slabs have no beams, column capitals or drop panels, which make formwork very simple and widely used, but the great disadvantage of flat plates or slabs supported by columns is that they are highly susceptible to punching shear failure under concentrated loads, compared with slabs supported by beams or walls.

In order to ensure the serviceability and strength requirements of such slabs, it is necessary to accurately predict their overall deformational characteristics throughout the range of their elastic and inelastic response as well as their strength at ultimate collapse. Although the need for experimental research to provide the basis for design equations continues, the development of powerful and reliable analytical techniques, such as finite element method, can, however, reduce the time and cost

[†] Corresponding Author, E-mail: msmadi@just.edu.jo

of otherwise expensive experimental tests, and may better simulate the loading and support conditions of the actual structure. Accurate results of finite element analysis, however, require adequate modeling of the actual behavior of reinforced concrete materials including nonlinearity. Reinforced concrete exhibits nonlinearity because of cracking, inelastic material behavior, stiffening and softening phenomena, complexity of bond between reinforcement and concrete and other factors (Chen and Saleeb 1982).

The derivation and implementation of various analytical finite element and materials models to investigate the structural and deformational behavior of reinforced concrete slabs and materials modeling has been the subject of many researches. However, the majority of these researches studied different behavioral aspects of normal strength concrete slabs (Vidoso, *et al.* 1988, Jiang and Mirza 1997, Reitman and Yankelevsky 1997, Polak 1998, 2005, Vainiunas, *et al.* 2004, Murray, *et al.* 2005, Deaton 2005) and others. This is not the case for high strength concrete, where very limited investigations have been carried out on the behavior of slabs (Marzouk and Chen 1993, Marzouk and Jiang 1996, Staller 2000, Salim and Sebastian 2002) and on other aspects of material modeling (Vecchio, *et al.* 1994, Shanmugam, *et al.* 2002, Fields and Bischoff 2004).

Through using a plasticity-based model and an 8-noded quadratic shell element with incorporating a realistic stress-softening relationships, Marzouk and Chen (1993) concluded that the post-cracking of high strength concrete has a significant effect on the entire load-deflection of high strength concrete slabs. In other finite element study by Marzouk and Jiang (1996) the enhancement of five types of shear reinforcement of high strength concrete plates was evaluated, and concluded that the double-bend, shear stud, and T-headed reinforcement were the most efficient shear reinforcements. Similar analytical studies using different finite element models was used by Staller (2000) and by Salim and Sebastian (2002) to predict the punching shear failure of normal and high strength concrete slabs.

The present study is part of this continuing effort to further explore the behavior of high strength concrete slabs through developing and implementing a three-dimensional nonlinear finite element program with proper materials models. Elasto-plastic work-hardening model, using 20-noded isoparametric brick element with embedded reinforcement is used. A suitable post-cracking model for high strength concrete is implemented to represent the retained post-cracking tensile stresses.

The FE formulation and material modeling is implemented in a finite element code in order to carry out the numerical study and to predict the behavior up to ultimate conditions of various slabs under transverse loads. The performance of slabs is evaluated in terms of load-deflection characteristics, concrete strains, and steel stresses. The validity and calibration of the theoretical formulations and the program used is judged through comparison of analytical results with available experimental data. Finally, a parametric study is carried out to investigate the influence of different material and geometric properties on the behavior of slabs.

2. Research significance

Although large amounts of analytical and experimental studies are available on the behavior of normal strength concrete slabs, limited number of finite element investigations have been carried out on slabs having higher strength concrete. In this paper, appropriate material nonlinearity models of high strength concrete including compression-softening and tension-stiffening phenomenon with proper failure criteria for concrete plates and shells is investigated. The models are implemented into a finite element program to provide the strength and deformational characteristics of companion

concrete slabs under variety of parameters and boundary conditions. Comprehensive data related to load-deflection curve, and stress and strain distribution is also provided.

3. Modeling of concrete material in compression

The behavior of concrete in compression is simulated by an elastic-plastic work hardening model up to onset of crushing. Generally, according to incremental theory of plasticity, the total strain increment is usually assumed to be the sum of elastic strain and plastic strain.

The formulation of the constitutive relations in the work-hardening plastic model is based on three fundamental assumptions (Chen and Saleeb 1982, Kwak and Filippou 1990, Al-Shaarbaf 1990, Crisfield 1994): The shape of the initial yield surface (failure criteria), the evolution of the hardening rule and formulation of an appropriate flow rule. However, the plasticity model and its constituent, and the modeling of concrete under triaxial state of stress, will be discussed in terms of the following elements with concentration on the difference of NSC and HSC material behavior: 1) Uniaxial stress-strain relationship, 2) Failure criterion, 3) Hardening rule, 4) Flow rule, and 5) Crushing condition.

3.1. Uniaxial stress-strain relationship

Frequently, the widely used stress-strain relationship of concrete up to the peak stress is given as a parabolic relationship as follows (Foster, *et al.* 1996, Pang and Hsu 1996, Bahn and Hsu 2000, Wang and Hsu 2001):

$$\sigma = f'_c \left[\frac{2\varepsilon}{\varepsilon_0} - \left(\frac{\varepsilon}{\varepsilon_0} \right)^2 \right] \quad (1)$$

Where ε_0 is the strain at peak stress f'_c given by

$$\varepsilon_0 = 2 \cdot \frac{f'_c}{E} \quad (2)$$

However, this equation failed to simulate the HSC and UHSC correctly. Therefore, a modified uniaxial stress-strain relationship is used in the present study which is composed of two parts; elastic linear part and parabolic part as shown in Fig. 1. A stress limit of $(\zeta \cdot f'_c)$ is used to separate the elastic and plastic portions of the curve, where the coefficient (ζ) represents the limit of elastic part and initiation of plastic deformation (Al-Shaarbaf 1990).

► For $\sigma \leq \zeta \cdot f'_c$, the linear part is given by:

$$\sigma = E \cdot \varepsilon_c \quad (3)$$

► For $\sigma > \zeta \cdot f'_c$, the parabolic part is given by:

$$\sigma = \zeta \cdot f'_c + E \left(\varepsilon_c - \frac{\zeta \cdot f'_c}{E} \right) - \left(\frac{E}{2 \cdot \varepsilon_0} \right) \left(\varepsilon_c - \frac{\zeta \cdot f'_c}{E} \right)^2 \quad (4)$$

Where: ε_c is the total strain, ε_0 is the total strain at peak stress which can be calculated

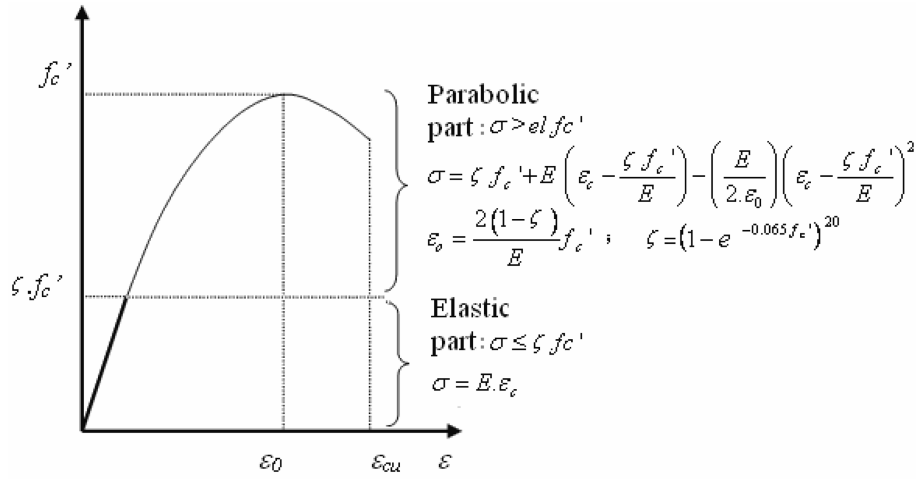


Fig. 1 Stress-strain relationship for concrete

$$\epsilon_0 = \frac{2(1-\zeta)}{E} f_c' \tag{5}$$

Based on best fitting of the linear parts of large number of concrete stress-strain properties of different grades presented by Attard and Stewart (1998) based on experimental data by Dahl (1992), the value of ζ is assumed to be dependent on the ultimate strength of concrete, and may be found using the following equation:

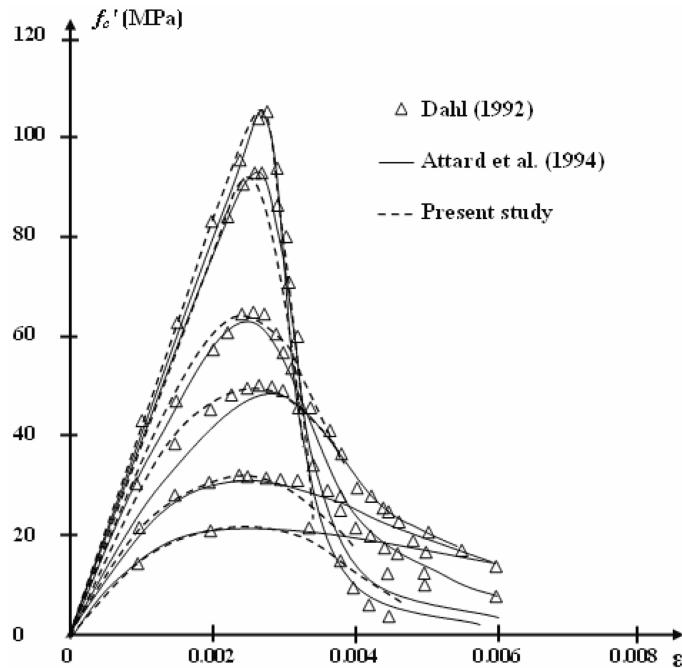


Fig. 2 Comparison of the proposed concrete stress-strain equation against other data

$$\zeta = (1 - e^{-0.065f'_c})^{20} \quad (6)$$

Fig. 2 indicates excellent agreement of the proposed uniaxial stress-strain model (Eq. 4) with the data presented by Attard and Stewart (1998) for normal, and high strength concrete. In the presence of orthogonal cracks which are caused by shear or transverse tensile stresses, concrete exhibits lower compressive strength and stiffness than uniaxially compressed state. Such degradation or softening in compressive strength of concrete is taken into consideration in the present study by multiplying the uniaxial compressive concrete stress defined by Eq. (4) by a softening factor $0 \leq \lambda \leq 1$ as shown in Fig. 3. Among various compression reduction models available in literature, the model suggested by Vecchio, *et al.* (1994), which takes into consideration the softening behavior of high strength concrete, is implemented in the present finite element formulation. The model can be expressed as:

$$\lambda = \frac{1}{1 + K_c \cdot K_f} \quad (7)$$

Where: K_c , represents the effect of the transverse cracking and straining, K_f represents the dependence on the strength of the concrete (f'_c), and are given by:

$$K_c = 0.27 \left(\frac{\varepsilon_r}{\varepsilon_0} - 0.37 \right) \quad (8)$$

$$K_f = 2.55 - 0.2629 \sqrt{f'_c} \leq 1.11 \quad (9)$$

Where: K_r is the tensile strain normal to the cracked plane given by:

- For cracked sampling point in the principal direction (①)

$$\varepsilon_r = \varepsilon_1 \quad (10)$$

For doubly cracked sampling point in both directions (①) and (②)

$$\varepsilon_r = (\varepsilon_1^2 + \varepsilon_2^2)^{\frac{1}{2}} \quad (11)$$

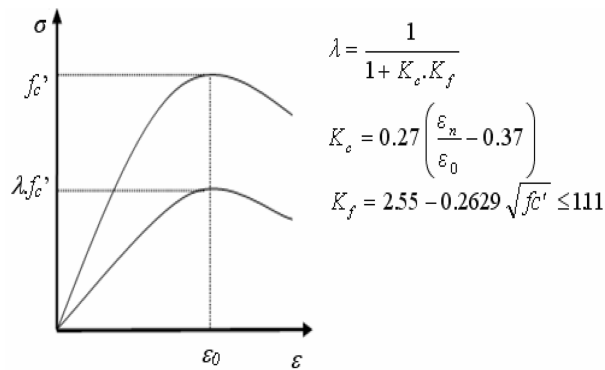


Fig. 3 Compression reduction of transversely cracked concrete

Where ε_1 is the transverse tensile strain in the principal direction (①) normal to the cracked plane, ε_2 is the tensile strain in the second direction (②) normal to the second crack plane.

3.2. Failure criterion

Under triaxial state of stress the failure criterion for concrete is generally assumed to be dependent on three stress invariants. However, the failure criterion used in this study is dependent on two stress invariants which has been proved to be adequate for most practical situations and has been successfully used by many investigators for analyzing reinforced concrete plate and shells (Figueiras and Owen 1984, Cervera and Hinton 1986, Naji 1989, Al-Shaarbaaf 1990) which can be expressed as:

$$f(\sigma) = f(I_1, J_2) = \sqrt{\alpha I_1 + 3\beta J_2} - \sigma_0 = 0 \quad (12)$$

Where

I_1 = the first stress invariant

J_2 = the second deviatoric stress invariant

σ_0 = the equivalent effective stress at the onset of plastic deformation.

$$\alpha = \sigma_0(\beta - 1) \quad (13)$$

$$\beta = \frac{1 - 2 \cdot \gamma}{\gamma^2 + 2 \cdot \gamma} \quad (14)$$

Noting that, for the equal biaxial compression state, the yield stress is given by

$$\sigma_x = \sigma_y = -\gamma\sigma_0 \quad (15)$$

Where γ is a constant to be determined from the biaxial failure envelop at stress ratio $\sigma_1/\sigma_2 = 1$. However, the constant was found by Hussein and Marzouk (2000) to have values of 19, 14 and 9% for f'_c of 42.7, 73.7 and 96.5 MPa, respectively (Fig. 4). Based on best fitting of these data the following equation for γ is suggested as function of f'_c :

$$\gamma = -(1.0782 \cdot 10^{-5}) \cdot f'_c{}^2 - (3.579 \cdot 10^{-4}) \cdot f'_c + 1.225 \quad (16)$$

3.3. The hardening rule and flow rule

An isotropic hardening rule is adopted in the present study which implies a uniform expansion of the initial yield surface without translation as plastic deformation increases. The required incremental stress-strain relationship may be obtained by differentiation of equivalent stress-strain relationship with respect to the plastic strain. This operation leads to the slope of the tangent of effective stress-plastic strain curve which represents the hardening coefficient, which is needed in the formulation of the incremental stress-strain relationship.

In order to calculate the plastic strain increment for a given stress increment, a flow rule must be defined. The associated flow rule has been widely used to concrete application by many researchers for reason of simplification (Al-Shaarbaaf 1990, Marzouk and Chen 1993), and it was adopted in the present study (Belakhdar 2006).

3.4. The crushing condition

The experimental tests of concrete under multiaxial loading indicate that the crushing is a strain related phenomenon (Chen and Saleeb 1982), so concrete is considered to crush when the strain reaches a specified ultimate value, after that the current stresses drop suddenly to zero and the concrete is assumed to lose its resistance completely against further deformation. Hence the crushing criterion is directly obtained by using the same form of yield criterion but in terms of strains, as follow (Al-Shaarbaf 1990):

$$\sqrt{\alpha \cdot I_1 + 3\beta \cdot J_2} = \epsilon_{cu} \tag{17}$$

Where

ϵ_{cu} : the ultimate concrete strain that can be obtained from the uniaxial compression test

If Eq. (17) is satisfied or the strain is grater than the specified ϵ_{cu} in this case the concrete is assumed to be crushed and the structure is ruptured, therefore the analysis stopped.

Frequently, the ultimate concrete crushing strain ϵ_{cu} is estimated to be in the range of 0.0030 as suggested by ACI-318-02 and NZS-95 codes to 0.0035 as given by BS8110 and CSA-94 codes. Based on experimental tests of singly reinforced concrete beams or eccentrically loaded columns without lateral confinement steel, the ultimate strain measured at the extreme compression face at failure was found to decrease as the ultimate compressive strength of concrete f'_c increases as shown in Fig. 5 (ACI Committee 363R-92 1997). Consequently, the value of the crushing strain ϵ_{cu} is taken as 0.0035 for normal strength concrete and 0.0030 for high strength concrete.

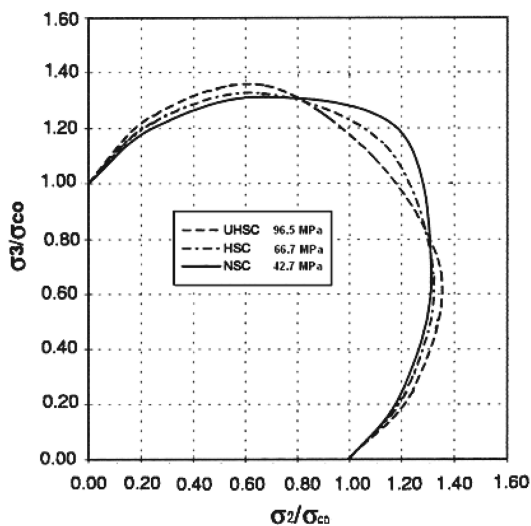


Fig. 4 Biaxial failure envelop of concrete (Hussein and Marzouk 2000)

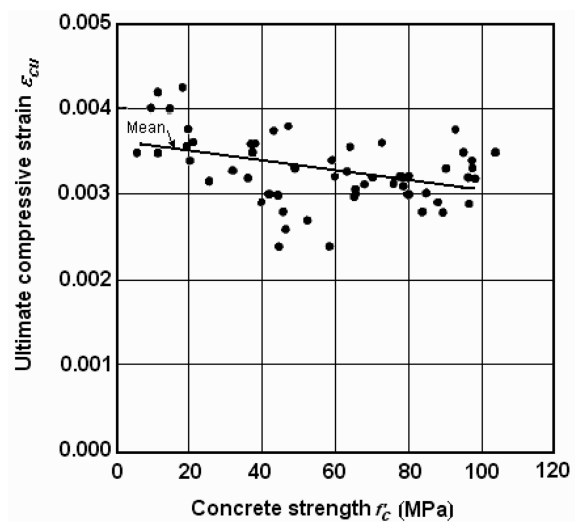


Fig. 5 Ultimate compressive strain versus compressive strength of concrete (ACI Committee 363R-92 1997)

4. Modeling of concrete materials in tension

When tensile stress exceeds a limiting value a crack is assumed to form in the plane perpendicular to the direction of that stress and concrete behaves no longer isotropic, and therefore, the normal stiffness is reduced through tension-stiffening concept. Once concrete has cracked, fixed smeared cracking model is used in the current study to model the crack. The gradual release of tensile stresses normal to the cracked plane may be represented by different types of average stress-strain curves to simulate the tension stiffening behavior. Although some of the tension stiffening models available in literature vary exponentially, the majority of models used in numerical analysis and implemented in finite element formulation are idealized as linear or bilinear curves (Sam and Lyer 1995, Staller 2000, Polak 2005) as follows:

► For $\varepsilon_{cr} \leq \varepsilon_n \leq \alpha_1 \varepsilon_{cr}$

$$\sigma_n = \alpha_2 \sigma_{cr} \left(\frac{\alpha_1 - \varepsilon_n}{\alpha_1 - 1} \right) \quad (18)$$

► For $\varepsilon_n > \alpha_1 \varepsilon_{cr}$

$$\sigma_n = 0 \quad (19)$$

Where:

σ_n, ε_n : are the stress and strain normal to the cracked plane

$\sigma_{cr}, \varepsilon_{cr}$: are the cracking stress and its corresponding cracking strain

α_1 : Parameter of tension stiffening which represents the rate of stress release as the crack widens.

α_2 : Parameter of tension stiffening which represents the sudden loss of stress at instant of cracking

The bilinear curve can also be simplified to linear curve by assuming that α_2 equals the to unity value. Bilinear tension-stiffening model is adopted in the present study as illustrated in Fig. 6.

The shear stiffness is also reduced when cracking occurs because it retains the two major mechanisms by which shear is transferred across the crack (the aggregate interlock of the rough crack surfaces and dowel action of the reinforcing bars crossing the crack planes). A bilinear shear retention model is used as shown in Fig. 7. This model consists of three parameters: (γ_1 : represents the rate of decay of shear stiffness as the crack widens, γ_2 : is the sudden loss in shear stiffness at the instant of cracking, and

γ_3 : is the residual shear stiffness due to the dowel action.). Besides, at onset of cracking Poisson's ratio (ν_c) is set to zero.

The material parameters used in the analysis are as follow:

– Tension stiffening: $\alpha_1 = 5, \alpha_2 = 0.6$

– Shear retention: $\gamma_1 = 10, \gamma_2 = 0.5, \gamma_3 = 0.04$

5. Material modeling of reinforcement

In contrast to concrete, the material modeling of steel is rather simple. Frequently, the steel is modeled using linear elastic-full plastic model, as shown in Fig. 8.

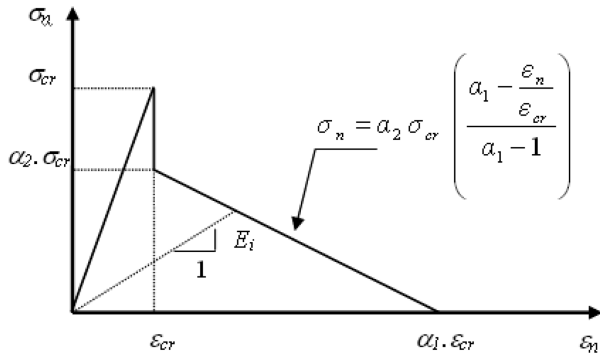


Fig. 6 Bilinear average tensile stress-strain of concrete

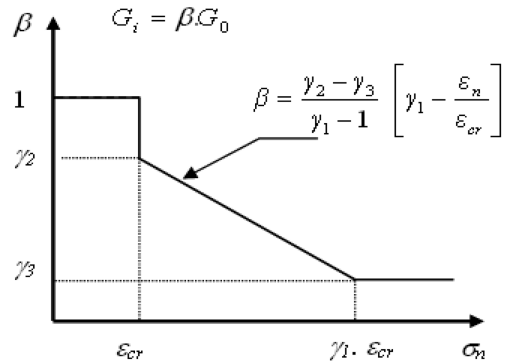


Fig. 7 Bilinear shear retention model

6. Finite element idealization

The concrete is represented by using 20-noded isoparametric brick element with total of sixty degrees of freedom as three translations at each node (u, v, w) in X, Y and Z directions respectively, and 27-integration rule ($3 \times 3 \times 3$). The reinforcing bars are modeled as one dimensional element subjected to axial force only embedded within the concrete brick elements and perfect bond is assumed to occur between the two materials, as shown in Fig. 9.

The non-linear equations of equilibrium have been solved using the incremental-iterative technique based on the modified Newton-Raphson method. The convergence of the solution was controlled by a load convergence criterion.

7. Validation of the analytical results

7.1. Description of selected experimental slabs

Eleven simply supported square slabs were selected from an experimental test of reinforced concrete slabs made of HSC and UHSC, to be used to validate and corroborate the predicted

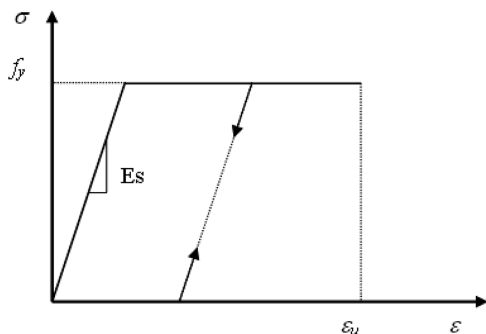


Fig. 8 Modeling of steel reinforcing bars

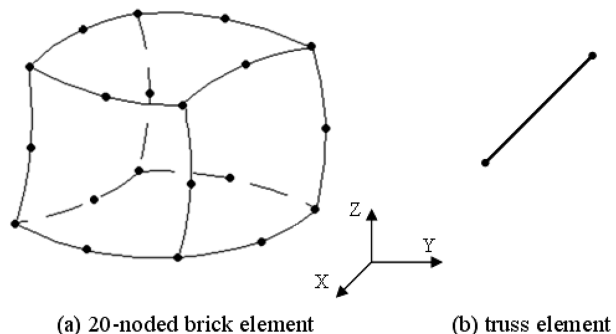


Fig. 9 Material idealization: (a): concrete element, (b): steel element

analytical results. The selected experimental slabs were carried out by Tomaszewicz (1993). All the selected slabs have span ranging between 1100 mm and 2500 mm, with thickness varies between 120 mm and 320 mm. The concrete compressive strength f'_c ranged from a minimum value of about 64 MPa to a maximum value of about 119 MPa. The steel ratio varied between 1.37% up to 2.34%. Thus, the selected slabs have satisfactory geometric and material variations in order to calibrate and test the efficiency and accuracy of the presented NLFE code. Additional information about material and geometric properties of these slabs are fully listed in Table 1. The following material properties are assumed in the analysis: $E_s = 200.000\text{MPa}$,

$$E_c = 3320 \cdot \sqrt{f'_c} + 6900, f_t = 33.0 \sqrt{f'_c}, \text{ and } \nu_c = 0.24.$$

7.2. Finite element mesh

By taking advantage of symmetry, a segment representing one quarter of the slabs has been considered in the finite element analysis, as shown in Fig. 10. The selected segment was modeled

Table 1 Slabs geometric and material properties

Ref	Slab	Clear span L (mm)	Slab thickness h (mm)	Effective depth d (mm)	Comp. strength f'_c (MPa)	Steel yield stress f_y (MPa)	Steel ratio ρ (%)
Tomaszewicz (1993)	ND65 -1-1	2500	320	300	64.30	500	1.37
	ND95 -1-1	2500	320	300	83.70	500	1.37
	ND95 -1-3	2500	320	300	89.90	500	2.29
	ND115-1-1	2500	320	300	112.00	500	1.37
	ND65 -2-1	2200	240	220	70.20	500	1.56
	ND95 -2-1	2200	240	220	88.20	500	1.56
	ND95 -2-3	2200	240	220	89.50	500	2.34
	ND95-2-3D	2200	240	220	80.30	500	2.34
	ND115-2-1	2200	240	220	119.00	500	1.56
	ND115-2-3	2200	240	220	108.10	500	2.34
	ND95 -3-1	1100	120	100	85.10	500	1.44

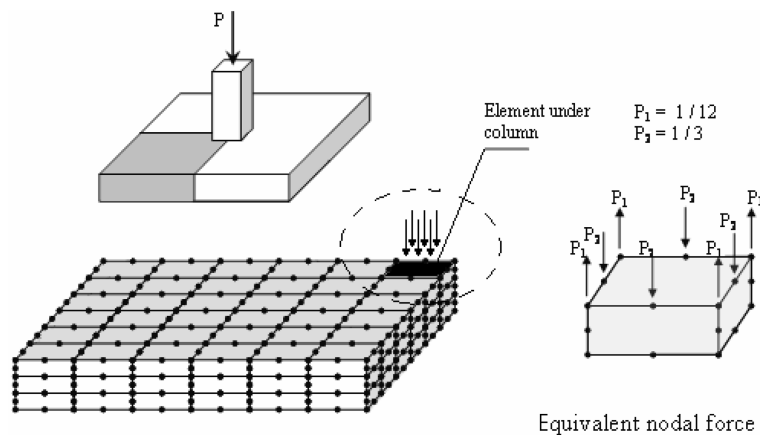


Fig. 10 Finite element mesh

using 20-node isoparametric brick elements, the model meshed to 108 elements with total of 679 nodes.

The load was applied carefully in small increments to prevent analysis problems and non-converged solution due to sudden cracking of concrete or yielding of reinforcements where the magnitude of load increment depends on the expected ultimate load (P_u) of the analyzed slab. The increment value ranged between 3% of P_u at the beginning of analysis and 0.5% of P_u in the second half of analysis.

7.3. Results of the analysis

The results of the present nonlinear finite element analysis of the investigated slabs using the modified program in terms of ultimate load, ultimate deflection and maximum steel strain are compared against the experimental measurements (Tomaszewicz 1993) and listed in Table 2. Fig. 11 shows typical load-deflection curves of selected slabs which show good agreement of the present finite element analysis and experimental results. Table 2 indicates that the predicted to experimental ultimate load ranges from 0.909 to 1.075 with standard deviation of 0.061, while the ultimate deflection ratio ranges from 0.681 to 1.006 with standard deviation of 0.098. Besides, the predicted bottom steel stress at failure to the experimental result ratio ranges from 0.816 to 1.194 with standard deviation of 0.115. According to Fig. 12, it can be observed that the present finite element model predicts the ultimate load of slabs accurately with very good agreement with experimental tests for concrete strength up to 119 MPa. Thus the present FE model performs satisfactory.

Table 2 Comparison of the predicted and experimental results

Slab	Experimental (Tomaszewicz 1993)			Present FE Analysis			FEA/Exp		
	Ultimate load P_u (KN)	Ultimate deflection D_u (mm)	Steel strain ε	Ultimate load P_u (kN)	Ultimate deflection D_u (mm)	Steel strain ε	P_u/P_u	D_u/D_u	ε/ε
ND65-1-1	2050	8.52	0.00165	1920	8.57	0.00185	0.937	1.006	1.123
ND95-1-1	2250	10.83	-	2340	9.98	0.00228	1.04	0.922	-
ND95-1-3	2400	7.97	0.00123	2580	7.89	0.00147	1.075	0.99	1.192
ND115-1-1	2450	11.65	0.00205	2540	10.29	0.00245	1.037	0.883	1.194
ND65-2-1	1200	9.61	0.00175	1120	7.53	0.00171	0.933	0.784	0.977
ND95-2-1	1100	9.28	0.00175	1160	7.34	0.00176	1.055	0.791	1.007
ND95-2-3	1450	9.73	0.00145	1480	7.48	0.00151	1.021	0.769	1.044
ND95-2-3D	1250	7.05	0.00140	1180	5.84	0.00114	0.944	0.828	0.816
ND115-2-1	1400	11.25	0.00216	1460	9.15	0.00223	1.043	0.813	1.032
ND115-2-3	1550	9.65	0.00150	1640	8.36	0.00168	1.058	0.866	1.118
ND95-3-1	330	7.81	0.00258	300	5.32	0.00252	0.909	0.681	0.977
						Ave	1.005	0.848	1.048
						St.Dev	0.061	0.098	0.115

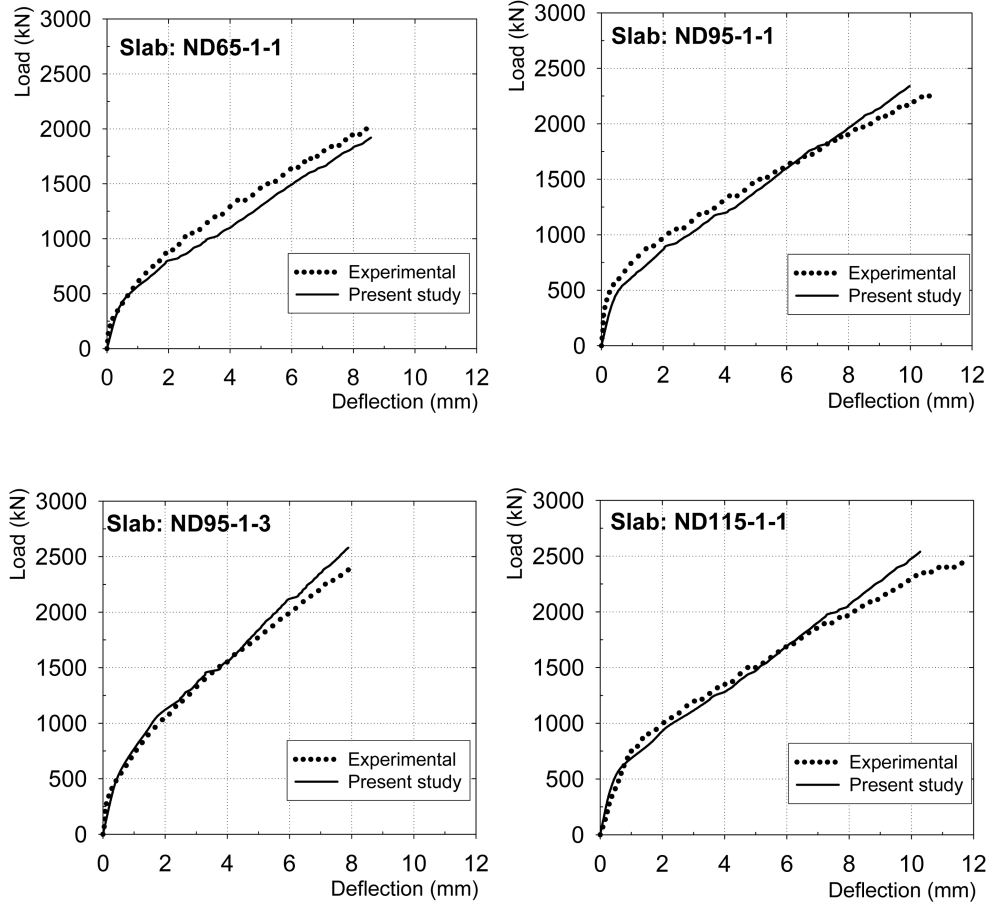


Fig. 11 Comparison of predicted and experimental load-deflection curves

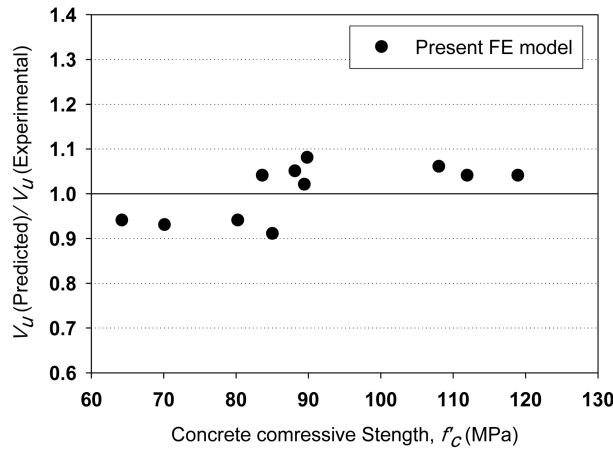


Fig. 12 Comparison of experimental and predicted ultimate load in terms of concrete strength

8. Parametric study on material properties

8.1. Effect of concrete compressive strength

The concrete compressive strength is considered as one of the important primary variables that were studied in the present finite element investigation on slab's behavior. The influence of different values of f'_c (25 N/mm² - 112 N/mm²) on the slab's ultimate load and ultimate deflection is shown in Fig. 13. It can be seen that both ultimate load and deflection increases as concrete strength increases. Agreement with experimental results is clearly indicated.

8.2. Effect of concrete tensile strength

The effect of tensile strength f_t on the behavior of slabs was studied using the following equations as shown in Fig. 14:

$$f_t = C\sqrt{f'_c} \tag{20}$$

Different values of the parameter C ranging from 0.33 to 0.70 were investigated. From the figure it can be seen that the ultimate strength increases as the parameter C increases, but the ultimate deflection is little influenced. Correct determination of the concrete tensile strength is very important in FE analysis, particularly in the post cracking stage. The above figure indicates that using $f_t = 0.33\sqrt{f'_c}$ gives the closest load-deflection relationship to experimental test results. Such finding agrees with conclusions by other researchers (Vecchio and Collins 1986, ACI Committee 435 1991, Chung and Ahmed 1994, Thabet and Haldane 2000).

8.3. Effect of reinforcement ratio

A numerical analysis was carried out using different values of steel ratio (ρ) ranging from 0.5 to

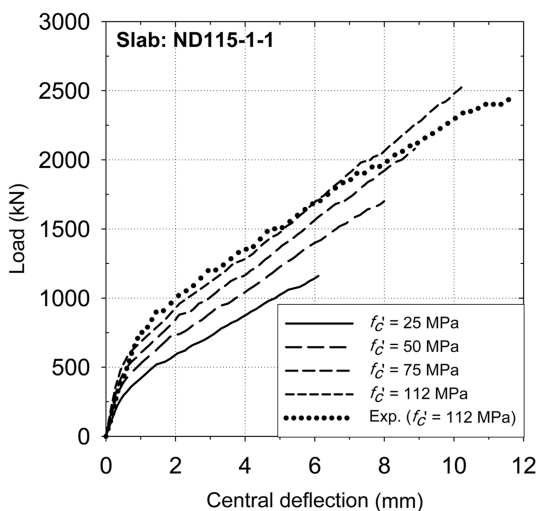


Fig. 13 Effect of the compressive strength on the slab response

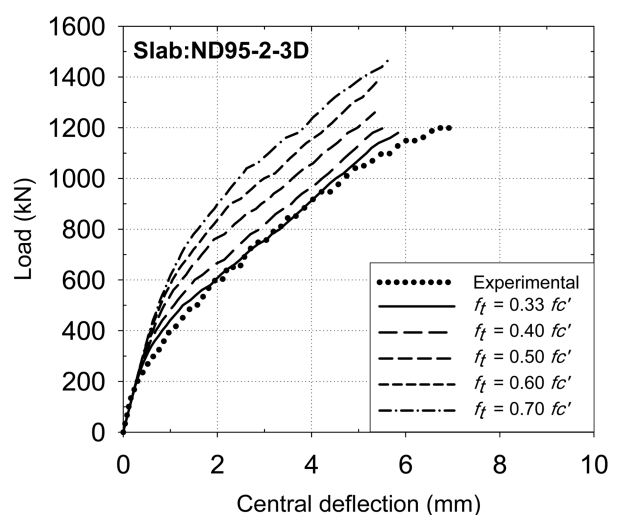


Fig. 14 Effect of tensile strength on the slab response

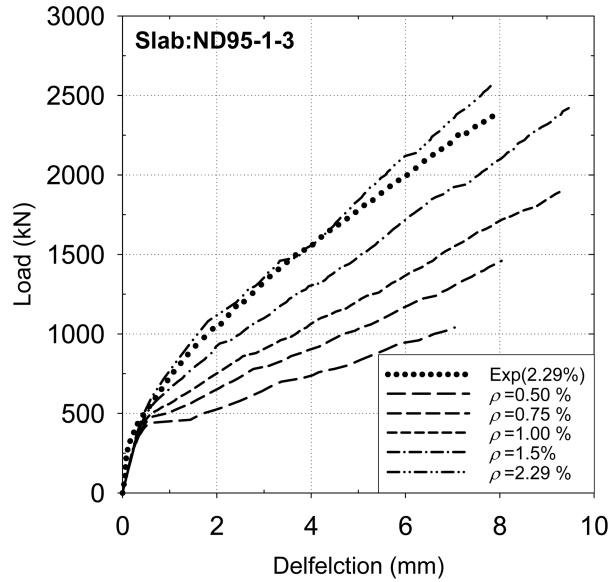


Fig. 15 Effect of reinforcement ratio on the load-deflection behavior

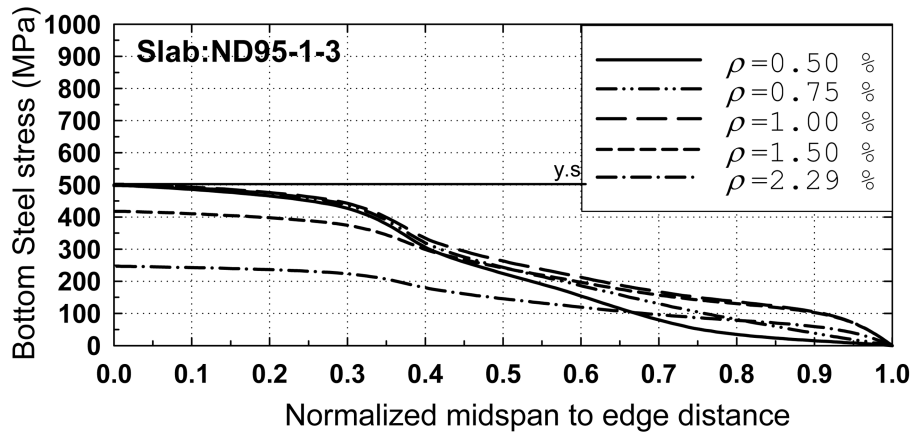


Fig. 16 Stress distribution of the reinforcement ratio on the bottom steel stress

2.29%, the results of which are shown in Fig. 15. It can be seen that prior to cracking, the steel ratio does not influence the load-deflection characteristics. However, after cracking ρ significantly influences the slab behavior, where both the ultimate load and deflection increases as the steel ratio increases. Furthermore, the slab stiffness as indicated from the slope of the load-deflection curve decreases as the steel ratio decreases. Such steel ratio alters the mode of failure from ductile behavior at small values of ρ to brittle behavior at higher values. Also, at lower value of ρ it has been observed that the yielding point is far from the ultimate point, and as ρ increases the yield point converges to the ultimate point until they become superposed, while at higher values of ρ , yielding may not takes place, as shown in the Fig. 16 which clarifies that the bottom steel at reinforcement ratio greater than 1.0% has not reached the yield stress (500 MPa).

8.4. Effect of span-to-depth ratio

To study the effect of span-to-depth ratio on slab behavior, the selected slabs were analyzed using different values of slab thickness which ranged from 120 mm to 320 mm, (span-to-depth ratio ranging from 8.33 to 25). The results obtained in terms of slab load-deflection relationships are presented in Fig. 17. Form this figure, it can be seen that the span-to-depth ratio has a great effect on the behavior and the load carrying capacity of the slab, where small increase in slab thickness leads to a significant increase in the ultimate load and reduction in deflection. When the span-to-depth ratio (s/d) decreases from 25 to 12.5, the ultimate load increases to about four times, but this increase becomes eight times at $s/d = 8.33$. Besides, the bottom steel stress at low values of s/d (≤ 16.6) are small and did not reach the yield stress, however, at high values of s/d (>16.6), only the reinforcement under or near the column face yielded, as shown in Fig. 18.

The top concrete strain distribution over the slab midspan at onset of failure is shown in Fig. 19 which indicates that the concrete strain increases as the span-to-depth ratio (s/d) increases and decreases with distance from midspan to the edge of slab. The maximum concrete strain (ϵ_{cu}) at the top fiber of slabs for s/d of 8.33, and 25 was about (-0.0015) and (-0.00278), respectively. As can be seen, the ultimate crushing strain of 0.003 was not reached at the top fibers in all slabs. However, according to the failure criterion adopted in the finite element formulation, the crushing strain of 0.003 will have been reached along the third principal strain axis, more likely beneath the column stub.

8.5. Effect of boundary conditions

Fig. 20 illustrates the behavior of high strength concrete slabs under different combinations of simply supported and fixed supports. It can be noticed that the supports conditions have a significant influence on the slab load-deflection behavior. As expected, the slab with fixed edges has higher load carrying capacity with smaller central deflection and lower ductility compared with others. Otherwise simply supported or column supported slabs with same properties carried a lower load with higher central deflection as shown in Fig. 21. More specifically, the load carried by fully

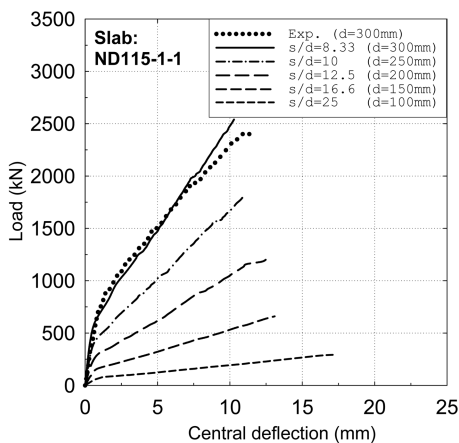


Fig. 17 Effect of span-to-depth ratio on HSC slabs behavior

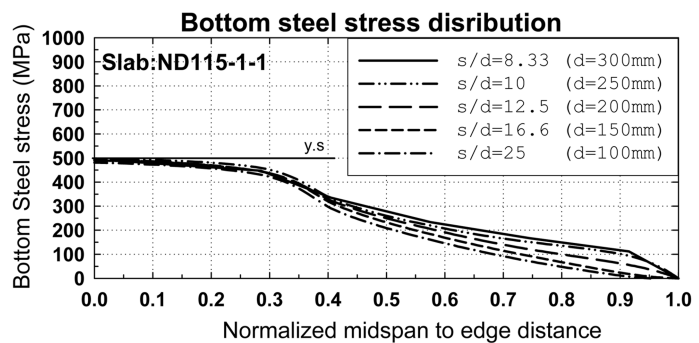


Fig. 18 Effect of span-to-depth ratio on mid-span steel-stress distribution

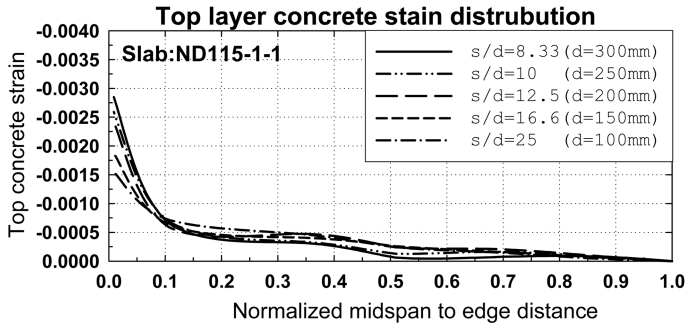


Fig. 19 Effect of span-to-depth ratio on concrete stain distribution

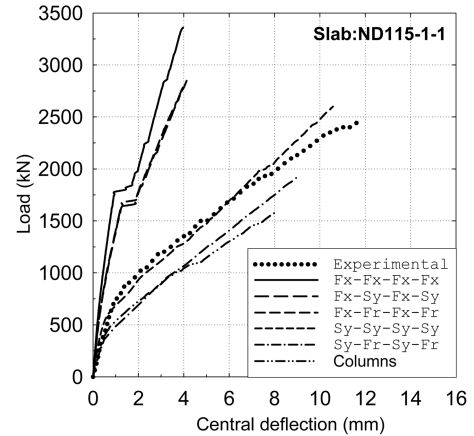


Fig. 20 Effect of boundary condition on HSC slab response

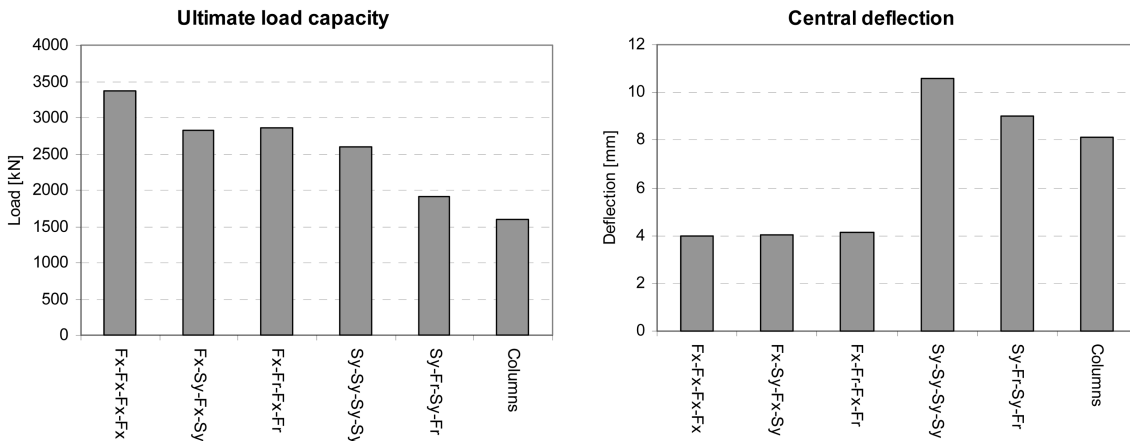


Fig. 21 Effect of boundary conditions on ultimate load capacity and corresponding deflection

fixed slab can attain to about 130% and 210% of the load carried by simply supported slab and column supported slab, respectively with corresponding deflection percentages equals to 40% and 50%, respectively.

9. Conclusions

A computer program suitable for nonlinear analysis of three dimensional reinforced concrete members under monotonic increasing loads has been developed to simulate the behavior of HSC and UHSC slabs. The concrete is represented by using 20-noded isoperimetric brick elements, while the reinforcing bars are modeled as one dimensional element embedded within the concrete brick elements. The nonlinear behavior of concrete in compression is simulated by an elastic-plastic work-hardening model up to onset of crushing. A linear-parabolic stress-strain curve has been used

to model the equivalent uniaxial stress-strain curve of concrete. In tension, a fixed smeared crack model has been used with tension-stiffening model. A shear retention models that modifies the shear stiffness, and softening models that reduce the concrete compressive strength, due to cracking are also implemented. The non-linear equations have been solved using the modified Newton-Raphson method.

The presented finite element code program is used for the analysis of HSC concrete slabs. Various aspects of slab behavior were predicted using proper materials models and NLFE program and compared with available experimental data. The comparison was judged to be very well, and the analytical formulations were capable of accurately predicting the total response and capacity of the concrete slabs. Material and geometric parametric-study was carried out to investigate the effect of different parameters on the slab's behavior.

There are several conclusions that may be drawn from the present study, which are related to the FE analysis and to the behavior of HSC slabs:

A) The part of the study concerning developing nonlinear finite element formulation to predict the response of high strength concrete slabs yields the following conclusions:

1-Nonlinear finite element method based on advanced 3D models is a powerful and relatively economical tool which can be effectively used to simulate the true behavior of reinforced concrete slabs even under complex conditions.

2-The choice of adequate material model for numerical simulation is the most important aspect in finite element modeling of concrete structures.

3-The proposed equation for the complete stress-strain diagram of concrete (Eq. 4) was proved to be applicable for all grades of concrete strength, and found to comply well with test data.

4-The tension stiffening and shear retention models have a considerable effect on the total behavior of high strength concrete slabs and their parameters can significantly improve the correlation of the predicted results with the experimental data.

5-The compression reduction factor (λ) (compression softening model) has small effect on the concrete slabs response and slightly affects the failure load.

B) The other part of study concerning the effect of material properties on slab behavior yields the following conclusions:

1-The slab capacity depends largely on the concrete strength, slab thickness, and reinforcement ratio. The amount of augmentation in slab capacity using higher strength concrete (HSC), increases as the slab thickness and reinforcement ration increases. However, using HSC in thin slabs with low reinforcement ratio has a small effect on slab ultimate load capacity, but increases the slab deflection.

2-Tensile strength affects the cracking load as well as the entire load-deflection curve and the failure load. Thus correct determination of the tensile strength of concrete is very important. In the present study, the best result was obtained using $f_t = 0.33\sqrt{f'_c}$

3-The span-to-depth ratio has a great effect on the behavior and the load carrying capacity of concrete slabs, where small increase in slab thickness leads to a significant increase in the ultimate load capacity and reduction in deflection.

4-The supports conditions have a significant influence on the slab load-deflection behavior. Slabs with fixed supports provide highest load capacity with lowest deflection, while highest deflection was obtained in slabs with simply supported edges and column supported slabs having the same properties.

Notation

α, β	= Material parameters of failure criterion
γ	= Constant of hydrostatic biaxial stress
α_1, α_2	= Tension-stiffening parameters
β	= Shear retention factor
E, E_c	= Modulus of elasticity of concrete
E_s	= Modulus of elasticity of reinforcement
ε	= Strain
ε_0	= Strain at peak stress
ε_{cr}	= Concrete cracking strain
ε_{cu}	= Concrete crushing strain
ε_e	= Elastic strain
ε_p	= Plastic strain
ε_n	= Strain normal to the crack surface
ε_u	= Ultimate strain
$f(\sigma)$	= Failure function
f_c	= Uniaxial compressive strength of concrete
f_y	= Steel yielding stress
G_0	= Original shear modulus
G_i	= Reduced shear modulus
η, η_2, η_3	= Shear retention parameters
I_1	= First stress invariant
J_2	= Second deviatoric stress invariant
K_c	= Transverse strain-related modification factor
K_f	= Concrete strength--related modification factor
λ	= Compressive strength reduction factor
ζ	= Plasticity limit coefficient
ρ	= Steel ratio
σ	= Stress
ν_c	= Poisson's ratio
σ_{cr}, f_t	= Cracking stress, concrete tensile strength
σ_n	= Stress normal to the crack surface

References

- ACI Committee 363R-92 (1997), "State-of-the-art report on high-strength concrete", (ACI 363R-92), 55.
- ACI Committee 435 (1991), "States of the art report on control of two way slab deflections", *ACI Struct. J.*, **88**(4), 501-514.
- Al-Shaarbaf, I. (1990), "Three-dimensional non-linear finite element analysis of reinforced concrete beams in torsion", PhD Thesis, University of Bradford.
- Attard, M. M. and Stewart, M. G. (1998), "A two parameter stress block for high-strength concrete", *ACI Struct. J.*, **95**(3), 305-317.
- Bahn, B. Y. and Hsu, T. T. C. (2000), "Cyclically and biaxially loaded reinforced concrete slender columns", *ACI Struct. J.*, **97**(3), 444-454.

- Belakhdar, K. A. M. (2006), "Three dimensional nonlinear finite element analysis of high strength reinforced concrete slabs", M.Sc Thesis, Faculty of Graduate Studies, Jordan University of Science and Technology, Irbid, Jordan, 188.
- Cervera, M. and Hinton, E. (1986), "Nonlinear analysis of reinforced concrete plates and shells using a three dimensional modeling of reinforced concrete structures", Pineridge Press, Swansea, UK, 327-370.
- Chen, W. F. and Saleeb, A. F. (1982), "Constitutive equations for engineering material", John Wiley & Sons, New York, V. 1, 580.
- Chung, W. and Ahmed, H. (1994), "Model for shear critical high strength concrete beams", *ACI Struct. J.*, **91**(1), 31-41.
- Crisfield, M. A. (1994), "Nonlinear finite element analysis of solids and structures", Department of Aeronautics, Imperial College of Science, Technology and Medicine, London, UK, John Wiley & Sons, v. 1, 345.
- Dahl, K. K. B. (1992), "Uniaxial stress-strain curves for normal and high strength concrete", ABK Report No.R282, Department of Structural Engineering, Technical University of Denmark.
- Deaton, J. B. (2005), "A finite element approach to reinforced concrete slab design", M.Sc Thesis, School of Civil and Environmental Engineering, Georgia Institute of Technology, 170.
- Fields, K. and Bischoff, P. (2004), "Tension stiffening and cracking of high-strength reinforced concrete tension members", *ACI Struct. J.*, **101**(4), 447-456.
- Figueiras, J. A. and Owen, R. J. (1984), "Nonlinear analysis of reinforced concrete shell structures", Proceedings of the International Conference on Computer Aided Analysis and Design of Concrete Structures, Yugoslavia.
- Foster, S. J., Budiono, B. and Gilbert, R. I. (1996), "Rotating Crack Finite Element Model For Reinforced Concrete Structures", *Comput. Struct.*, **58**(1), 43-50.
- Hussein, A. and Marzouk, H. (2000), "Behavior of high-strength concrete under biaxial stresses", *ACI Mater. J.*, **97**(1), 27-36.
- Jiang, J. and Mirza, F. (1997), "Nonlinear analysis of reinforced concrete slabs by discrete finite element approach", *Comput. Struct.*, **65**(4), 1667-1687.
- Kwak, H. G. and Filippou, F. C. (1990), "Finite element analysis of reinforced concrete structures under monotonic loads", Structure Engineering Mechanics and Materials, Report No.USB/SEMM-90/14, Department of Civil Engineering, University of California, Berkeley, 120.
- Marzouk, H. and Chen Z. (1993), Finite element analysis of high strength concrete slabs: *ACI Struct. J.*, **90**(5), 505-513.
- Marzouk, H. and Jiang, D. (1996), "Finite element evaluation of shear enhancement of high strength concrete plates", *ACI Struct. J.*, **93**(6), 667-673.
- Murray, K. A., Cleland, D. J. and Gilbert, S. (2005), "The development of non-linear numerical model to simulate the behaviour of reinforced concrete flat slabs in the vicinity of edge columns", *Construct. Bldg. Mater.*, **19**, 703-712.
- Naji, J. H. (1989), "Non-linear finite element analysis of reinforced concrete panels and infilled frames under monotonic and cyclic loading", PhD Thesis, University of Bradford.
- Pang, X. B. and Hsu, T. T. C. (1996), "Fixed angle softened truss model for reinforced concrete", *ACI Struct. J.*, **93**(2), 197-207.
- Polak, M. A. (2005), "Ductility of reinforced concrete flat slab-column connections", *Comput Aided Civ. Infrastruct. Eng.*, **20**, 184-193.
- Polak, M.A. (1998), "Modelling punching shear of reinforced concrete slabs using layered finite elements", *ACI Struct. J.*, **95**(1), 71-80.
- Reitman, M. and Yankelevsky, D. (1997), "A new simplified model for nonlinear RC slabs analysis", *ACI Struct. J.*, **94**(4), 399-408.
- Salim, W. and Sebastian, W. (2002), "Plasticity model for predicting punching shear strengths of reinforced concrete slabs", *ACI Struct. J.*, **99**(6), 827-835.
- Sam, C. and Lyer, P. K. (1995), "Nonlinear finite element analysis of reinforced concrete four pile caps", *Comput. and Struct.*, **57**(4), 605-622.
- Shanmugam, N. E., Kumar, G. and Thevendram, V. (2002), "Finite element modeling of double skin composite slabs", *Fin. Elements in Anal. and Des.*, **38**, 579-599.
- Staller, D. (2000), "Analytical studies and numerical analysis of punching shear failure in reinforced concrete

- slabs”, *TRITA-BKN Bulletin*, **57**, 8.
- Thabet, A. and Haldane, D. (2000), “Three-dimensional simulation of nonlinear response of reinforced concrete members subjected to impact loading”, *ACI Struct. J.*, **97**(5), 698-702.
- Tomaszewicz, A. (1993), “High-strength concrete”, SP2 (Plates and Shells, Report 2.3, Punching Shear Capacity of Reinforced Concrete Slabs; Report No. STF70A93082); SINTEF, Trondheim, 36.
- Vainiunas, P., Popovas, V. and Vilnius, A. J. (2004), “Nonlinear FEA of RC floor slab-to-column joint connection”, Theoretical Foundations of Civil engineering-XII, Ed. by W. Szczesninak, OW PW, Warsaw, 12.
- Vecchio, F. and Collins, M. (1986), “The modified compression field theory for reinforced concrete element subjected to shear”, *ACI J.*, **83**(2), 219-231.
- Vecchio, F., Collins, M. and Aspiotis, J. (1994), “High strength concrete elements subjected to shear”, *ACI Struct. J.*, **91**(4), 423-433.
- Vidoso, F., Kotsovos, M. and Pavlovic, M. (1988), “Symmetrical punching of reinforced concrete slabs: an analytical investigation based on NFE modelling”, *ACI Struct. J.*, **85**(2), 241-250.
- Wang, T. and Hsu, T. C. C. (2001), “Nonlinear finite element analysis of concrete structures using new constitutive models”, *Comput. Struct.*, **79**, 2781-2791.

CC